Available online at www.sciencedirect.com
ScienceDirect
Physics Letters A 372 (2008) 3801–3807
PHYSICS LETTERS A
www.elsevier.com/locate/pla

Tunneling in quantum superlattices with variable lacunarity

Francisco R. Villatoro [a], Juan A. Monsoriu [b,*]

[a] *Departamento de Lenguajes y Ciencias de la Computación, Universidad de Málaga, E-29071 Málaga, Spain*
[b] *Departamento de Física Aplicada, Universidad Politécnica de Valencia, E-46022 Valencia, Spain*

Received 10 October 2007; received in revised form 25 February 2008; accepted 6 March 2008

Available online 8 March 2008

Communicated by R. Wu

Abstract

Fractal superlattices are composite, aperiodic structures comprised of alternating layers of two semiconductors following the rules of a fractal set. The scattering properties of polyadic Cantor fractal superlattices with variable lacunarity are determined. The reflection coefficient as a function of the particle energy and the lacunarity parameter present tunneling curves, which may be classified as vertical, arc, and striation nulls. Approximate analytical formulae for such curves are derived using the transfer matrix method. Comparison with numerical results shows good accuracy. The new results may be useful in the development of band-pass energy filters for electrons, semiconductor solar cells, and solid-state radiation sources up to THz frequencies.

PACS: 03.65.Nk; 05.45.Df

Keywords: Fractal potential; Polyadic Cantor set; Transfer matrix method; Quantum scattering

1. Introduction

Quantum superlattices are microelectronic devices composed of alternating layers of two semiconductors with different energy band gaps deposited over a substrate [1–4]. The sandwiching of two materials whose band gap energies are different results in a rectangular potential well for the electrons (holes) in the conduction (valence) band. The thickness of each semiconductor layer is about 10–100 atoms (1–10 nm), so this three-dimensional finite potential well may be split into a two-dimensional system in the transversal dimensions, where electrons behave as a two-dimensional electron gas with continuous energy states, and a one-dimensional finite square well in the growth direction with discrete bound states.

The scattering in semiconductor superlattices can be easily solved by means of the transfer matrix method using an effective mass for the electrons [5–10]. In fact, in the absence of external electric fields, semiconductor superlattices may be considered, in a first approximation, as a quasi-one-dimensional system of rectangular quantum wells separated by potential barriers. The "effective mass" (m^*) accounts for the external forces applied to the electrons in the quantum-well heterostructure, since they do not respond as free particles due to the influence of other atoms.

Fractal superlattices have been experimentally developed by alternating semiconductor materials according to an iterative fractal process using techniques such as molecular beam epitaxy [11–13]. These devices may be crystalline or amorphous. A typical device of the first kind consists of several layers of gallium arsenide (GaAs) sandwiched between aluminium gallium arsenide ($Al_xGa_{1-x}As$) ones, where the crystal composition x may vary between 0 and 1, such as those fabricated by Axel and Terauchi [14] using $x = 0.3$, corresponding to a monolayer of $Al_xGa_{1-x}As$ with thickness of 0.28 nm. A typical amorphous device is made by alternating layers of amorphous germanium (a-Ge) and amorphous silicon (a-Si) deposited in a silicon substrate, as the polyadic Cantor superlattices experimentally grown by Järrendahl et al. [15] in which each layer has a thickness less than 1.4 nm with good sharpness. Numer-

* Corresponding author.
E-mail address: jmonsori@fis.upv.es (J.A. Monsoriu).

0375-9601/$ – see front matter
doi:10.1016/j.physleta.2008.03.002

ical results neglect the effects due to fabrication imperfections in order to simplify the analysis. The comparison with experimental results, as those for triadic Cantor superlattices with 3^6 elementary layers [15], show that the biggest imperfections, small layer thickness fluctuations, and interface mixing, mainly influence the peak intensity, but the relative peak positions are much less affected. Hence, theoretical analysis and experimental results compare reasonably well, stressing the usefulness of the first ones for the development of new microelectronic devices in practical applications [13].

In this Letter, the scattering of electrons in symmetrical polyadic Cantor fractal potentials, characterized by a lacunarity parameter which is independent of their fractal dimension, is studied by means of a simple analytical model. The authors have shown in Ref. [16], by means of a numerical implementation of the transfer matrix method, that the representation of the reflection coefficient as a function of the particle energy and the lacunarity shows perfectly transparent tunneling along some curves, referred to as nulls, which may be classified as vertical (lacunarity-independent), arc (concave upward), and striation (concave downward) nulls. In an optical context, Ref. [17] presents similar results. The goal of this Letter is the detailed derivation from first principles of analytical expressions for the reflection-less energies of particles in fractal superlattices designed as polyadic Cantor sets with variable lacunarity.

In applications of fractal superlattices as electron pass-band filters, the introduction of lacunarity as a new design parameter, which adds to the fractal dimension and the stage of growth of the fractal, allows one to minimize the pass-band insertion loss and to adjust the center frequency of the filter [18,19]. In photovoltaics, the highly fragmented band structure of fractal superlattices may overcome the limit efficiency of current semiconductor solar cells [20,21]. Let us emphasize that, in practical devices, the experimental lacunarity parameter is discrete, an integer multiple of the thickness of a monoatomic layer of the material, instead of a continuous one, introducing a limitation which has to be properly taken into account. However, ferromagnetic/superconductor and superconductor/superconductor, cuprate based oxide superlattices which allow spatial modulations having an energy-independent incommensurate periodicity, referred to as supermodulation [22], may be used to experimentally develop continuous lacunarity superlattices, although no one has been experimentally developed up to the present.

The contents of this Letter are as follows. Section 2 recalls the characteristics of symmetrical, polyadic, Cantor fractal superlattices. Section 3 presents the analytical formulas for the reflection-less energies, whose validity is shown in Section 4 by comparisons with numerical results. Finally, Section 5 summarizes the main conclusions.

2. Polyadic Cantor superlattices

In Cantor superlattices, the distribution of the layers' thickness along the growth axis corresponds, in a finite order approximation, to a polyadic, or generalized, Cantor set [24,25]. These sets are defined as follows. The first step ($S = 0$) is to take a segment of unit length, referred to as the initiator. In the next step, $S = 1$, the segment is replaced by N non-overlapping copies of the initiator, each one scaled by a factor $\gamma < 1$. For N odd, as shown in Fig. 1(a), one copy lies exactly centered in the interval, and the remaining ones are distributed such that $\lfloor N/2 \rfloor$ copies are placed completely to the left of the interval and the remaining $\lfloor N/2 \rfloor$ copies are placed wholly to its right, where $\lfloor N/2 \rfloor$ is the greatest integer less than or equal to $N/2$; additionally, each copy among these $N-1$ ones is separated by a fixed distance, let us say ε. For N even, as shown in Fig. 1(b), one half of the copies is placed completely to the left of the interval and the other half completely to its right, with each copy separated by ε. At the following construction stages of the fractal set, $S = 2, 3, \ldots$, the generation process is repeated over and over again for each segment in the previous stage. Strictly speaking, the Cantor set is the limit of this procedure as $S \to \infty$, which is composed of geometric points distributed so that each point lies arbitrarily close of other points of the set, being the Sth stage Cantor set usually referred to as a pre-fractal or physical fractal.

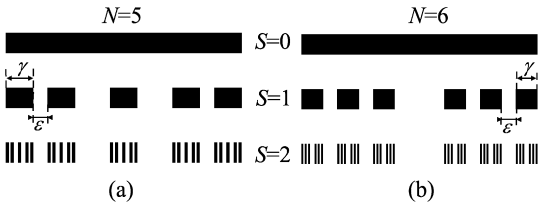

Fig. 1. First two stages ($S = 1$ and $S = 2$) of polyadic Cantor fractal sets with $N = 5$ (a) and $N = 6$ (b), showing the definition of both the scale factor (γ) and the lacunarity parameter (ε). Black and white regions denote the potential values $-V$ and 0, respectively.

Symmetrical polyadic Cantor fractals are characterized by three parameters, the number of self-similar copies N, the scaling factor γ, and the width of the outermost gap at the first stage, ε, here on referred to as the lacunarity parameter, as in most of the previous technical papers dealing with polyadic Cantor fractals in engineering applications [17,26]. The similarity dimension of all polyadic Cantor fractals is $D = \ln(N)/\ln(\gamma^{-1}) = -\ln(N)/\ln(\gamma)$, which is independent of the lacunarity parameter. The three parameters of a polyadic Cantor set must satisfy certain constraints in order to avoid overlapping between the copies of the initiator. On the one hand, the maximum value of the scaling factor depends on the value of N, such that $0 < \gamma < \gamma_{\max} = 1/N$. On the other hand, for each N and γ, there are two extreme values for ε. The first one is $\varepsilon_{\min} = 0$, for which the highest lacunar fractal is obtained, i.e., that with the largest possible gap. For N even, the central gap has a width equal to $1 - N\gamma$, and, for N odd, both large gaps surrounding the central well have a width of $(1 - N\gamma)/2$. The other extreme value is

$$\varepsilon_{\max} = \begin{cases} \frac{1-N\gamma}{N-2}, & \text{even } N, \\ \frac{1-N\gamma}{N-3}, & \text{odd } N, \end{cases}$$

where for even (odd) N two (three) wells are joined together in the center, without any gap in the central region. The width of the $N-2$ gaps in this case is equal to $\varepsilon_{\max}$. Thus, the corresponding lacunarity is lower than that for $\varepsilon = 0$, but not the

smallest one, which is obtained for the most regular distribution, where the gaps and wells have the same width at the first stage ($S = 1$) given by

$$\varepsilon_{\text{reg}} = \frac{1 - N\gamma}{N - 1}.$$

Note that $0 < \varepsilon_{\text{reg}} < \varepsilon_{\max}$.

3. Estimation of the null positions

The graphical representation of the scattering reflection coefficient as a function of both the particle energy and the lacunarity parameter for polyadic Cantor pre-fractal potentials, referred to as a twist plot, presents a characteristic null structure (black lines and curves) corresponding to energies at which the particle transparently tunnels through the fractal potential wells, i.e., for which the reflection coefficient is nil.

The reflection coefficient nulls may be separated in three main families. The first and most noticeable is the family of vertical nulls, being caused by the bound states of the particle in each potential well, and, thus independent of the lacunarity parameter. The nulls in the second family, denoted as arc nulls, are concave upward and curve from the upper left to the lower right of the twist plots. The third family of nulls, referred to as striation nulls, form the finer structure of the twist plots being curves which are concave downward, running from the lower left to the upper right of each twist plot.

3.1. Transfer matrix method

The scattering problem for polyadic Cantor sets with variable lacunarity can be easily solved by means of the transfer matrix method using an effective mass for the electrons. Let us summarize the main details of this widely known technique.

The quantum scattering of particles in one-dimensional potential wells is governed by the steady-state, linear Schrödinger equation

$$-\frac{\hbar^2}{2m^*}\frac{d^2\psi(x)}{dx^2} + V(x)\psi(x) = E\psi(x), \tag{1}$$

where $\psi(x)$, m^* and E are the particle wavefunction, effective mass and energy, respectively, $\hbar$ is Planck's constant, and $V(x)$ describes a distribution of potential wells, taken as a piecewise constant function, here on. The wavefunction ψ_i in the region where the potential constant value is V_i, is the sum of two plane waves, $\psi_i(x) = \psi_i^+(x) + \psi_i^-(x)$, given by

$$\psi_i^{\pm}(x) = A_i^{\pm} e^{\pm \mathrm{i} k_i x}, \quad k_i = \frac{1}{\hbar}\sqrt{2m^*(E - V_i)},$$

where $\mathrm{i} = \sqrt{-1}$, k_i is the local particle momentum, and $A_i^{\pm}$ are integration constants to be determined by applying the standard boundary conditions at the interfaces between successive wells. In this Letter, a distribution of potential wells of the same depth is considered, so the potential $V_i = -V$ in the wells and $V_i = 0$ outside them.

The solution of Eq. (1) for a distribution of N constant potential wells is easily obtained by means of the transfer matrix method [6–9,23], yielding

$$\begin{pmatrix} A_0^+ \\ A_0^- \end{pmatrix} = M \begin{pmatrix} A_{N+1}^+ \\ A_{N+1}^- \end{pmatrix}, \tag{2}$$

where

$$M = D_0^{-1}\left(\prod_{i=1}^{N} D_i P_i(d_i) D_i^{-1}\right) D_{N+1},$$

$$D_i = \begin{pmatrix} 1 & 1 \\ k_i & -k_i \end{pmatrix}, \; P_i(d_i) = \begin{pmatrix} e^{\mathrm{i}k_i d_i} & 0 \\ 0 & e^{-\mathrm{i}k_i d_i} \end{pmatrix},$$

where d_i is the width of the ith potential well.

Both the reflection and transmission coefficients of the scattering of a quantum particle, incoming from the left, with the N-well potential is determined by the coefficients of the matrix M,

$$\begin{pmatrix} A_0^+ \\ A_0^- \end{pmatrix} = \begin{pmatrix} M_{11} & M_{12} \\ M_{21} & M_{22} \end{pmatrix} \begin{pmatrix} A_{N+1}^+ \\ 0 \end{pmatrix},$$

where no backward particle can be found on the right side of the potential, so $A_{N+1}^- = 0$. Both the reflection and transmission coefficients [27] are given by

$$R = \frac{|A_0^-|^2}{|A_0^+|^2} = \frac{|M_{21}|^2}{|M_{11}|^2}, \qquad T = \frac{|A_{N+1}^+|^2}{|A_0^+|^2} = \frac{1}{|M_{11}|^2}, \tag{3}$$

respectively, since $k_{N+1} = k_0$.

3.2. Vertical nulls

The vertical nulls shown in the twist plots are the result of bound states of the particle due to its resonance on every potential well of the Cantor superlattice. Since there are N^S potential wells at the Sth stage pre-fractal, the vertical nulls are very noticeable in the twist plot. Using the transfer matrix method, it is easy to calculate their exact positions.

Let us consider a quantum well at the Sth stage pre-fractal whose width is $a = L\gamma^S$, where L is the length of the initiator, separated from the next one by a distance $b = L\epsilon^S = a(\epsilon/\gamma)^S$. For future convenience, let us take a symmetrical configuration in which the quantum well is surrounded by two regions of width $b/2$, which corresponds to $V_0 = V_2 = 0$, $V_1 = -V$, $d_1 = a$, and $d_0 = d_2 = b/2$, in the notation introduced in Section 3.1. The particle momentum at the three constant potential regions may be normalized as

$$k_0 = k_2 = \frac{\sqrt{2m^*E}}{\hbar} = \frac{\phi}{a},$$

$$k_1 = \frac{\sqrt{2m^*(E+V)}}{\hbar} = \frac{\sqrt{\phi^2 + \phi_V^2}}{a}, \tag{4}$$

where ϕ and ϕ_V are the (non-dimensional) particle energy and depth of the potential well, respectively. The total scattering matrix is given by

$$M = P_0(b/2) D_0^{-1} D_1 P_1(a) D_1^{-1} D_0 P_2(b/2) = \begin{pmatrix} M_{11} & M_{12} \\ M_{21} & M_{22} \end{pmatrix}, \tag{5}$$

which may be easily calculated to obtain

$$M_{11} = M_{22}^* = e^{ibk_0}\left(\cos(ak_1) + i\frac{k_0^2+k_1^2}{2k_0k_1}\sin(ak_1)\right),$$

$$M_{12} = M_{21}^* = -i\frac{k_0^2-k_1^2}{2k_0k_1}\sin(ak_1),$$

where the asterisk indicates complex conjugate.

The vertical nulls correspond to bound states of the particle inside the potential well, being characterized by a nil reflection coefficient, for which Eq. (3) yields

$$\sin(ak_1) = \sin\left(\sqrt{\phi^2+\phi_V^2}\right) = 0,$$

having countably infinite solutions given by

$$\sqrt{\phi_i^2+\phi_V^2} = i\pi, \quad i = 1, 2, \ldots. \tag{6}$$

Note that the position of the vertical nulls is independent of both the initiator length and the pre-fractal stage thanks to the normalization of the energy (4).

3.3. Arc nulls

The arc nulls are caused by collective bound states of the particle in any of the $2N^{S-1}$ copies of the series of $\lfloor N/2\rfloor$ potential wells wholly on either the right or left side of each of the N^{S-1} copies of the initiator at the Sth stage of the pre-fractal superlattice. Since these collective bound states depend on the distance between individual wells, they are a function of the lacunarity parameter.

The Cayley–Hamilton theorem [28] states that every matrix M satisfies the equation given by its characteristic polynomial which for a 2×2 matrix is given by $p_M(\lambda) = \lambda^2 - \mathrm{tr}(M)\lambda + \det(M)$, where $\mathrm{tr}(M)$ and $\det(M)$ are the trace and determinant, respectively, of the matrix. For the scattering matrix of a potential well, Eq. (5), which is a unitary matrix, $\det(M) = |M_{11}|^2 + |M_{12}|^2 = 1$, and $\mathrm{tr}(M) \in \mathbb{R}$. Without loss of generality, $\mathrm{tr}(M) = 2\cos(\theta)$, where θ is the Bloch phase, being a real number if $|\mathrm{tr}(M)| \leqslant 2$ and a complex one otherwise, and purely imaginary only if $\mathrm{tr}(M) > 0$. Therefore, the Cayley–Hamilton theorem yields

$$M^2 = 2\cos(\theta)M - I,$$

where I is the identity matrix. This equation allows the calculation of the nth power of the matrix M as

$$M^n = \frac{\sin(n\theta)}{\sin(\theta)}M - \frac{\sin((n-1)\theta)}{\sin(\theta)}I, \tag{7}$$

which can be easily proved by the induction principle; note that

$$\begin{aligned} M^{n+1} &= MM^n \\ &= \frac{\sin(n\theta)}{\sin(\theta)}\big(2\cos(\theta)\big)M - \frac{\sin(n\theta)}{\sin(\theta)} - \frac{\sin((n-1)\theta)}{\sin(\theta)}M, \end{aligned}$$

and use the formula $2\cos(\theta)\sin(n\theta) = \sin((n+1)\theta) + \sin((n-1)\theta)$. The off-diagonal element $(M^n)_{21}$ of Eq. (7) is

$$\big(M^n\big)_{21} = \frac{\sin(n\theta)}{\sin(\theta)}M_{21},$$

hence the reflection coefficient is nil for

$$\sin(n\theta) = 0, \qquad \sin(\theta) \neq 0, \tag{8}$$

whose countably infinite solutions are the set of Bloch phases given by

$$n\theta_{ij} = (ni + j)\pi, \quad i = 0, 1, 2, \ldots, \ j = 1, 2, \ldots, n-1, \tag{9}$$

where $n = \lfloor N/2\rfloor$ in our case. Note that, in the right-hand side of this expression, π appears multiplied by all the natural numbers except the multiples of n, for which $\sin(n\theta)/\sin(\theta) = n$.

The Bloch phase may be calculated from Eq. (5) which yields

$$\begin{aligned} \mathrm{tr}(M) &= 2\cos(bk_0)\cos(ak_1) - \frac{k_0^2+k_1^2}{k_0k_1}\sin(bk_0)\sin(ak_1) \\ &= \frac{(k_0+k_1)^2}{2k_0k_1}\cos(bk_0+ak_1) \\ &\quad - \frac{(k_0-k_1)^2}{2k_0k_1}\cos(bk_0-ak_1). \end{aligned}$$

Eq. (4) yields $ak_0 = \phi$ and

$$ak_1 = \sqrt{\phi^2+\phi_V^2} = \phi + \frac{1}{2}\left(\frac{\phi_V}{\phi}\right)^2 + \mathcal{O}\left(\left(\frac{\phi_V}{\phi}\right)^4\right),$$

so for $\phi \gg \phi_V$, $k_0 \approx k_1$ and

$$\mathrm{tr}(M) = 2\cos(\theta) = 2\cos(ak_1 + bk_0) + \mathcal{O}\big((k_1-k_0)^2\big). \tag{10}$$

Therefore, from Eq. (9), the normalized energy ϕ_{ij} for the arc nulls may be calculated as function of the lacunarity as

$$\begin{aligned} &\sqrt{\phi_{ij}^2+\phi_V^2} + \left(\frac{\varepsilon}{\gamma}\right)^S\phi_{ij} = \left(i + \frac{j}{\lfloor N/2\rfloor}\right)\pi, \\ &\quad i = 0, 1, 2, \ldots, \ j = 1, 2, \ldots, \lfloor N/2\rfloor - 1. \end{aligned} \tag{11}$$

Note also that

$$\begin{aligned} \sin(n\theta) &= \sin\big(n\arccos\big(\mathrm{tr}(M)/2\big)\big) \\ &= \frac{\sqrt{4-\mathrm{tr}(M)^2}}{2}U_n\big(\mathrm{tr}(M)/2\big), \end{aligned}$$

where $U_n(x)$ is the nth Chebyshev polynomial of the second kind [7]. The value of this expression at the arc nulls is straightforwardly checked since

$$\mathrm{tr}(M) = 2\cos(\theta_{ij}) = 2(-1)^j,$$

where Eq. (9) has been used.

3.4. Striation nulls

The striation nulls are caused by the quantum interference between the $\lfloor N/2\rfloor$ potential wells on the right with those on the left side in each of the N^{S-1} copies of the initiator at the Sth stage of the pre-fractal superlattice. This interaction is exact for N even and only approximate for N odd due to the presence of the potential well at the center of each copy of the initiator. Obviously, they also are a function of the lacunarity parameter.

Let us start with the N even case. Let c be the distance between the rightmost potential well of the $\lfloor N/2\rfloor$ wells on the left

and the leftmost one of those at the right in every copy of the initiator at the Sth stage, yielding $c = L(1 - N\gamma^S - (N-2)\varepsilon^S)$. The scattering matrix for this problem is $\tilde{M}^2$ where

$$\tilde{M} = P_0(c/2)M^{\lfloor N/2\rfloor}P_0(c/2).$$

Eqs. (8) and (9) for $n = 2$ yield

$$2\tilde{\theta}_i = (2i+1)\pi, \quad i = 0, 1, 2, \ldots,$$

where $\mathrm{tr}(\tilde{M}) = 2\cos(\tilde{\theta})$, which may be easily calculated from

$$\mathrm{tr}(\tilde{M}) = \mathrm{tr}\big(M^{\lfloor N/2\rfloor}\big)\,\mathrm{tr}\big(P_0(c)\big).$$

Introducing the trace operator into Eq. (7) yields

$$\mathrm{tr}\big(M^n\big) = \frac{\sin(n\theta)}{\sin(\theta)}\mathrm{tr}(M) - 2\frac{\sin((n-1)\theta)}{\sin(\theta)} = 2\cos(n\theta),$$

hence, using Eq. (10), for $\phi \gg \phi_V$,

$$\mathrm{tr}(\tilde{M}) = 2\cos\big(n(ak_1 + bk_0)\big)2\cos(ck_0) + \mathcal{O}\big((k_1 - k_0)^2\big),$$

yielding $\tilde{\theta} \approx nak_1 + (nb + c)k_0$, where $n = \lfloor N/2\rfloor$, and resulting in

$$\lfloor N/2\rfloor\sqrt{\phi_i^2 + \phi_V^2} + \left(\gamma^{-S} - N - \big(N - \lfloor N/2\rfloor - 1\big)\left(\frac{\varepsilon}{\gamma}\right)^S\right)\phi_i = (2i+1)\frac{\pi}{2}, \quad i = 0, 1, 2, \ldots, \tag{12}$$

for the striation nulls for N even.

For the N odd case, the central potential well between both series of $\lfloor N/2\rfloor$ wells makes their mutual interference not exact. However, an approximate formula may be obtained as easily as before. Let $c = L(1 - N\gamma^S - N\varepsilon^S)$ such that $c/2 + b$ is the distance between the central potential well and that in the right (or left) in every copy of the initiator at the Sth stage. The corresponding scattering matrix is $\hat{M}^2$ where

$$\hat{M} = P_1(a/2)D_1^{-1}D_0P_0(c/2)M^{\lfloor N/2\rfloor}P_0(c/2)D_0^{-1}D_1P_1(a/2),$$

where the central potential well has been divided in two parts, one located completely to the left and the other one completely to the right. By exactly the same arguments as before, omitted here for brevity, $\mathrm{tr}(\hat{M}) = 2\cos(\hat{\theta})$, where

$$\hat{\theta} \approx \big(N - \lfloor N/2\rfloor\big)(ak_1 + bk_0) + ck_0,$$

resulting in

$$\big(N - \lfloor N/2\rfloor\big)\sqrt{\phi_i^2 + \phi_V^2} + \left(\gamma^{-S} - N - \big(\lfloor N/2\rfloor - 1\big)\left(\frac{\varepsilon}{\gamma}\right)^S\right)\phi_i = (2i+1)\frac{\pi}{2}, \quad i = 0, 1, 2, \ldots, \tag{13}$$

as an approximation for the striation nulls for N odd. Note that Eq. (12) is a particular case of Eq. (13), being valid for both even and odd N.

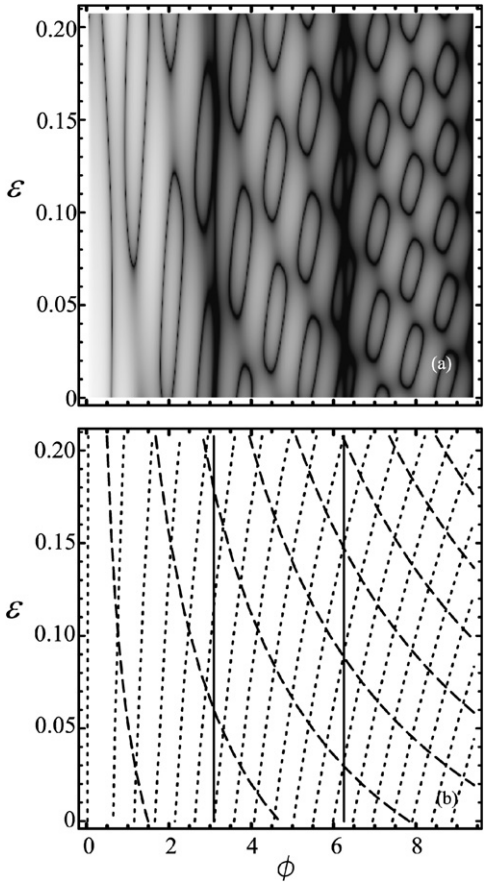

Fig. 2. Scattering reflection coefficient (a) for the polyadic Cantor pre-fractal potentials with $S = 1$, $N = 5$, $\gamma = 1/7$, and $\phi_V = 1/2$, and the analytical curves (b) for the corresponding vertical (continuous line), arc (dashed line), and striation (dotted line) nulls.

4. Presentation of results

Twist plots are the gray-scale representation of the scattering reflection coefficient (in decibels, i.e., $10\log_{10} R$) as a function of the normalized energy (ϕ) and the lacunarity parameter (ε). Here, a linear gray scale was used, from black for nil values to white for the maximum value equal to unity. Figs. 2(a) and 3(a) show twist plots for, respectively, pentadic ($N = 5$) and hexadic ($N = 6$) Cantor fractal potentials both with $S = 1$, $\gamma = 1/7$, and $\phi_V = 1/2$. The horizontal interval covers the normalized energy ϕ from 0 to $\sqrt{(3\pi)^2 - \phi_V^2} \approx 9.41$, the energy of the third vertical null line. These figures have been obtained by a straightforward numerical implementation of the transfer matrix method.

The most noticeable fact in Figs. 2(a) and 3(a) is the null structure (black lines and curves) corresponding to energies at which the particle transparently tunnels through the fractal potential wells. The darkest curves are the vertical nulls. The arc nulls, which are concave upward, curving from the upper left to the lower right of the plots, appear in pairs for $N = 6$ (see Fig. 3(a)), as expected from Eq. (11). The striation nulls, which are concave downward, running from the lower left to the upper right of each twist plot, form the finer structure of the twist plots.

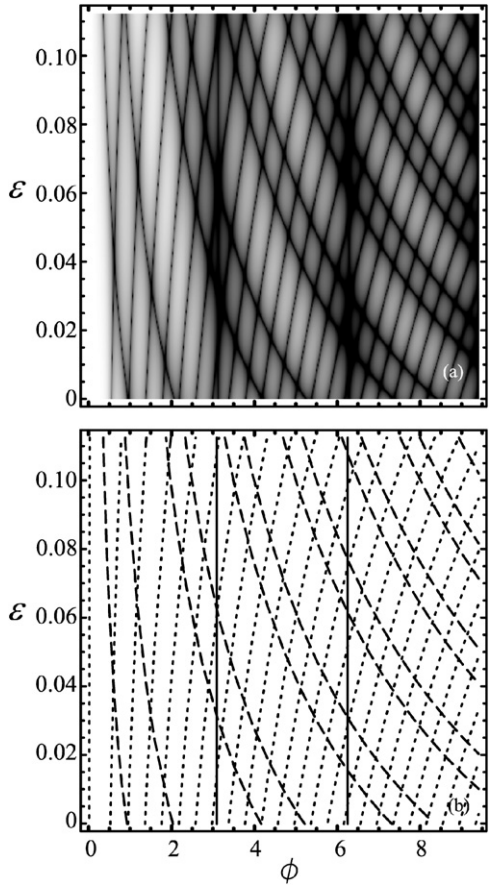

Fig. 3. Scattering reflection coefficient (a) for the polyadic Cantor pre-fractal potentials with $S = 1$, $N = 6$, $\gamma = 1/7$, and $\phi_V = 1/2$, and the analytical curves (b) for the corresponding vertical (continuous line), arc (dashed line), and striation (dotted line) nulls.

The main difference between Figs. 2(a) and 3(a) is observed for $N = 5$ and, in general, for N odd, because, in such a case, the tunneling is not perfectly transparent trough the whole length of both the arc and the striation nulls, resulting in a leopard-like spot pigmentation pattern. This result is not unexpected, since both the arc and the striation nulls are not truly nil for N odd due to the single quantum well between each pair of $\lfloor N/2 \rfloor$ potential wells, which introduces non-periodicity in the scattering problem and thus results in a (small) non-nil reflection coefficient.

The nulls calculated by Eqs. (6), (11), and (13), for $S = 1$, $\gamma = 1/7$, and $\phi_V = 1/2$, are shown in Figs. 2(b) and 3(b). The comparison of these figures with those shown in Figs. 2(a) and 3(a), respectively, clearly illustrates the good accuracy of the analytical approximations obtained in this Letter, which reproduce the main features of the corresponding twist plots. For N even, the accuracy is surprisingly good. For N odd, as expected, both arc and striation nulls are less accurate. Note also that the accuracy degrades for small energy as expected due to the lack of validity of the approximations used in Sections 3.3 and 3.4 in such a case.

For higher stages of growth of the polyadic Cantor fractal, not shown here for brevity, finer null patterns appear in the twists plots which also are very well accounted for by the analytical expressions derived in this Letter.

5. Conclusions

Simple analytical expressions for the calculation of the particle energy for transparent tunneling in polyadic Cantor prefractal potentials as a function of the lacunarity parameter have been obtained from first principles by using the transfer matrix method. The comparison with the results obtained by a numerical implementation of the transfer matrix method shows the good accuracy of these expressions for N-adic Cantor prefractals with N even and their reasonable accuracy for N odd. The reasons for this difference in accuracy have also been presented in detail.

The transfer matrix methods may be adapted to the propagation of waves in general one-dimensional quasi-periodic media [29], therefore, the present method may be also applied to, for example, acoustics, optics, or vibrating strings. In fact, the effect of the lacunarity in the scattering on generalized Cantor media was extensively studied in optics [17,26], where the additional degree of freedom introduced by the lacunarity was used with success to obtain new physical characteristics. A detailed study of these applications, which are outside the scope of this Letter, may also be a topic for further study.

Acknowledgements

The authors acknowledge the suggestions of an anonymous reviewer which have improved the physical motivation of the Letter. This work has been supported by the Generalitat Valenciana (grant GV/2007/239), Spain. We also acknowledge the financial support from the Universidad Politécnica de Valencia, Programa de Apoyo a la Investigación y Desarrollo (PAID-06-07), Spain, and Project FIS2005-03191 from DGI-MEC, Spain.

References

[1] B.R. Nag, Physics of Quantum Well Devices, Springer, Berlin, 2002.
[2] P. Roblin, High-Speed Heterostructure Devices: From Device Concepts to Circuit Modeling, Cambridge Univ. Press, Cambridge, UK, 2002.
[3] R.M. Kolbas, N. Holonyak Jr., Am. J. Phys. 52 (1984) 431.
[4] R. Mazurczyk, Chaos Solitons Fractals 10 (1999) 1971.
[5] M. Nawrocki, J.A. Gaj, Am. J. Phys. 52 (1984) 807.
[6] T.M. Kalotas, A.R. Lee, Eur. J. Phys. 12 (1991) 275.
[7] D.W.L. Sprung, H. Wu, J. Martorrell, Am. J. Phys. 61 (1993) 1118.
[8] D.W.L. Sprung, J.D. Sigetich, H. Wu, J. Martorrell, Am. J. Phys. 68 (2000) 715.
[9] J.S. Walker, J. Gathright, Am. J. Phys. 62 (1994) 408.
[10] T.P. Horikis, Phys. Lett. A 359 (2006) 345.
[11] M.A. Herman, H. Sitter, Molecular Beam Epitaxy: Fundamentals and Current Status, Springer, Berlin, 1989.
[12] E.L. Albuquerque, M.G. Cottam, Phys. Rep. 376 (2003) 225.
[13] E. Maciá, Rep. Prog. Phys. 69 (2006) 397.
[14] F. Axel, H. Terauchi, Phys. Rev. Lett. 66 (1991) 2223.
[15] K. Järrendahl, M. Dulea, J. Birch, J.-E. Sundgren, Phys. Rev. B 51 (1995) 7621.
[16] J.A. Monsoriu, F.R. Villatoro, M.J. Marín, J. Pérez, L. Monreal, Am. J. Phys. 74 (2006) 831.
[17] A.D. Jaggard, D.L. Jaggard, J. Opt. Soc. Am. A 15 (1998) 1626.

[18] E. Diez, F. Domínguez-Adame, E. Maciá, A. Sánchez, Phys. Rev. B 54 (1996) 16792.
[19] A.S. Saleh, H. Aubert, Microw. Opt. Tech. Lett. 28 (2001) 127.
[20] R.W. Peng, M. Mazzer, K.W.J. Barnham, Appl. Phys. Lett. 83 (2003) 770.
[21] A.C. Varonides, Renew. Energy 33 (2008) 273.
[22] M. Vershinin, S. Misra, S. Ono, Y. Abe, Y. Ando, A. Yazdani, Science 303 (2004) 1995.
[23] J.A. Monsoriu, F.R. Villatoro, M.J. Marín, J.F. Urchueguía, P. Fernández de Córdoba, Eur. J. Phys. 26 (2005) 603.
[24] A.J. Hurt, Am. J. Phys. 56 (1988) 969.
[25] B.B. Mandelbrot, The Fractal Geometry of Nature, Freeman, New York, 1983.
[26] J.A. Monsoriu, G. Saavedra, W.D. Furlan, Opt. Express 12 (2004) 4227.
[27] R. Liboff, Introductory Quantum Mechanics, Benjamin Cummings, Redwood City, CA, 2003.
[28] C. Meyer, Matrix Analysis and Applied Linear Algebra, SIAM, Philadelphia, PA, 2001.
[29] D.J. Griffiths, C.A. Steinke, Am. J. Phys. 69 (2001) 137.